Monthly Notices
of the
ROYAL ASTRONOMICAL SOCIETY

MNRAS **448,** 3325–3338 (2015) doi:10.1093/mnras/stv214

Submillimetre observations of *WISE*/radio-selected AGN and their environments

Suzy F. Jones,[1⋆] Andrew W. Blain,[1] Carol Lonsdale,[2] James Condon,[2] Duncan Farrah,[3] Daniel Stern,[4] Chao-Wei Tsai,[4] Roberto J. Assef,[5] Carrie Bridge,[6] Amy Kimball,[7] Mark Lacy,[2] Peter Eisenhardt,[4] Jingwen Wu[8] and Tom Jarrett[9]

[1]*XROA, Department of Physics and Astronomy, University of Leicester, University Road, Leicester LE1 7RH, UK*
[2]*National Radio Astronomy Observatory, 520 Edgemont Road, Charlottesville, VA 22903-2475, USA*
[3]*Department of Physics MC 0435, Virginia Polytechnic Institute and State University, 850 West Campus Drive, Blacksburg, VA 24061, USA*
[4]*Jet Propulsion Laboratory, California Institute of Technology, 4800 Oak Grove Dr., Pasadena, CA 91109, USA*
[5]*Núcleo de Astronomía de la Facultad de Ingeniería, Universidad Diego Portales, Av. Ejército Libertador 441, Santiago, Chile*
[6]*California Institute of Technology MS249-17, Pasadena, CA 91125, USA*
[7]*CSIRO Astronomy & Space Science, PO Box 76, Epping, NSW 1710, Australia*
[8]*Division of Physics & Astronomy, University of California Los Angeles, Physics and Astronomy Building, 430 Portola Plaza, Los Angeles, CA 90095-1547, USA*
[9]*Astronomy Department, University of Cape Town, Rondebosch 7701, Republic of South Africa*

Accepted 2015 January 28. Received 2015 January 15; in original form 2014 November 27

ABSTRACT

We present JCMT SCUBA-2 850 μm submillimetre (submm) observations of 30 mid-infrared (mid-IR) luminous active galactic nuclei (AGNs), detected jointly by the *Wide-field Infrared Survey Explorer* (*WISE*) all-sky IR survey and the NVSS/FIRST radio survey. These rare sources are selected by their extremely red mid-IR spectral energy distributions (SEDs) and compact radio counterparts. Further investigations show that they are highly obscured, have abundant warm AGN-heated dust and are thought to be experiencing intense AGN feedback. These galaxies appear to be consistent with a later AGN-dominated phase of merging galaxies, while hot, dust-obscured galaxies are an earlier starburst-dominated phase. When comparing the number of submm galaxies detected serendipitously in the surrounding 1.5 arcmin to those in blank-field submm surveys, there is a very significant overdensity, of order 5, but no sign of radial clustering centred at our primary objects. The *WISE*/radio-selected AGN thus reside in 10-Mpc-scale overdense environments that could be forming in pre-viralized clusters of galaxies. *WISE*/radio-selected AGNs appear to be the strongest signposts of high-density regions of active, luminous and dusty galaxies. SCUBA-2 850 μm observations indicate that their submm fluxes are low compared to many popular AGN SED templates, hence the *WISE*/radio-selected AGNs have either less cold and/or more warm dust emission than normally assumed for typical AGN. Most of the targets are not detected, only four targets are detected at SCUBA-2 850 μm, and have total IR luminosities $\geq 10^{13}$ $L_{\odot}$, if their redshifts are consistent with the subset of the 10 SCUBA-2 undetected targets with known redshifts, $z \sim 0.44$–2.86.

Key words: galaxies: active – galaxies: clusters: general – galaxies: high-redshift – quasars: general – infrared: galaxies – submillimetre: galaxies.

1 INTRODUCTION

A popular galaxy evolution theory is for major mergers between gas-rich galaxies to cause tidal interactions between the two galaxies and gas is driven into the central regions of the galaxies (Sanders et al. 1988; Barnes & Hernquist 1992; Schweizer 1998; Farrah et al. 2001; Veilleux, Kim & Sanders 2002; Hopkins et al. 2006, 2008; Volonteri, Natarajan & Gültekin 2011). Gas is converted quickly into stars in a period of intense starburst activity ($<10^9$ yr), which dominates the luminosity. The active galactic nuclei (AGNs) are fuelled and merge, and with the increased gas supply can accrete at close to or above the Eddington rate (Assef et al. 2014), dominating the luminosity for a time as a powerful obscured AGN, and then

⋆ E-mail: sfj8@le.ac.uk

perhaps an optically bright quasar. Feedback from the supermassive black hole (SMBH) and supernovae can expel all the gas from the galaxy, and quench further star formation and BH accretion, leaving behind a passive elliptical galaxy. Hence, AGN feedback likely plays a crucial role in galaxy evolution. There are two modes for AGN feedback: radiative or wind mode, it is intense and short-lived ($\ll 10^8$ yr), when the accreting BH is close to the Eddington limit and affects the distribution of cold gas (Farrah et al. 2012), and the second is kinetic or maintenance mode, which lasts longer and is less intense than radiative mode, it is jet-driven, and is when the galaxy has a hot halo (Fabian 2012). From previous observations, radiative mode feedback is important for highly luminous, obscured galaxies, comparable to the galaxies observed in this paper, and kinetic mode feedback is important in nearby massive elliptical galaxies (Fabian 2012). However, a combination of both radiative and jet-driven feedback modes could be important for the targets of this paper, because the galaxies are extremely luminous and obscured, and also contain radio jets. Observations of AGN feedback, especially at the peak epoch of cosmic star formation, $z \sim 2$–3, are required to fully understand how AGN feedback affects the host galaxy.

To observe AGN feedback in action, mid-infrared (mid-IR) selections are very successful (de Grijp, Lub & Miley 1987; Low et al. 1988; Sanders et al. 1988; Spinoglio & Malkan 1989; Keel et al. 1994; Lacy et al. 2004; Stern et al. 2005, 2012; Yan et al. 2005; Polletta et al. 2006, 2008; Gruppioni et al. 2008; Sacchi et al. 2009; Tommasin et al. 2010; Donley et al. 2012; Assef et al. 2013; Mateos et al. 2013). NASA's *Wide-field Infrared Survey Explorer* (*WISE*; Wright et al. 2010) is able to find luminous, dusty, high-redshift, active galaxies because the hot dust heated by AGN and/or starburst activity can be traced using the *WISE* 12 μm (*W*3) and 22 μm (*W*4) bands. Eisenhardt et al. (2012), Bridge et al. (2012, 2013) and Lonsdale et al. (submitted) have shown that *WISE* can find different classes of interesting, luminous, high-redshift, dust-obscured AGN. There has been previous work on heavily-obscured, hyperluminous, *WISE*-selected AGNs from Eisenhardt et al. (2012), Wu et al. (2012), Jones et al. (2014) and Tsai et al. (2014) who observed galaxies with faint or undetectable flux densities in the 3.4 μm (*W*1) and 4.6 μm (*W*2) bands, and well-detected fluxes in the *W*3 and/or *W*4 bands, but a radio blind selection. These galaxies, which also host obscured AGNs, are called '*W*1*W*2-dropouts' or hot, dust-obscured galaxies (Hot DOGs; Wu et al. 2012; Jones et al. 2014). Hot DOGs are thought to be consistent with a later, transient phase of a major merger compared to submillimetre galaxies (SMGs; Jones et al. 2014), and a comparison of submillimetre (submm) observations of the *WISE*/radio-selected AGNs and their surrounding environments are presented in this paper, to see if they are different.

The observations of luminous, dusty, high-redshift, active galaxies also revealed significant evidence that the galaxy density in the environments of high-redshift far-IR and mid-IR luminous galaxies appears to be above average (Blain et al. 2004; Borys et al. 2004; Farrah et al. 2006; Scott, Dunlop & Serjeant 2006; Gilli, Comastri & Hasinger 2007; Chapman et al. 2009; Hickox et al. 2009, 2012; Cooray et al. 2010). Clustering of these mid-IR and SMGs could be evidence for massive dark matter haloes and highlight bias of this distribution as compared with the underlying dark matter distribution. There is also evidence that SMGs are found in dense environments from Umehata et al. (2014), who observed the protocluster SSA22 field with the Astronomical Thermal Emission Camera (AzTEC) on the Atacama Submillimeter Telescope Experiment (ASTE), at 1.1 mm to a depth of 0.7–1.3 mJy beam^{-1}, and found 10 SMGs correlated with $z = 3.1$ Lyman-alpha emitters in the protocluster. There is also evidence for high-redshift radio galaxies (HzRGs) to reside in overdense regions as traced by dusty galaxies (Stevens et al. 2003, 2010; Falder et al. 2010; Galametz et al. 2010, 2012; Mayo et al. 2012; Wylezalek et al. 2013, 2014; Hatch et al. 2014). This suggests that HzRGs are progenitors of massive galaxies in the centre of rich galaxy clusters in the present-day Universe (Stevens et al. 2003, 2010; Venemans et al. 2007; Falder et al. 2010; Galametz et al. 2010, 2012; Mayo et al. 2012; Wylezalek et al. 2013; Hatch et al. 2014): in particular, the *Herschel* Galaxy Evolution Project (HeRGÉ) found that the HzRG MRC 1138−26 at $z = 2.156$, the Spiderweb galaxy, is a protocluster environment (Seymour et al. 2012). Further evidence is from the Clusters Around Radio-Loud AGN (CARLA) *Spitzer* programme that looked at the environments of radio-loud AGN (RLAGN) at $1.2 < z < 3.2$, and concluded that RLAGN are in overdense environments in mid-IR wavelengths, and could be signposts of high-redshift galaxy clusters (Wylezalek et al. 2013; Hatch et al. 2014). Donoso et al. (2014) looked at ∼170 000 *WISE*-selected Hot DOGs and found that obscured AGN are found in denser environments than unobscured AGN. Stevens et al. (2003) observed seven HzRGs with Submillimetre Common-User Bolometer Array (SCUBA), and compared the number of serendipitous sources in the fields of seven HzRGs and their lambda cold dark matter (ΛCDM) simulation predicted distribution (fig. 4), and showed the data and simulations show that either no companions or two companions are found in the HzRG fields. Stevens et al. (2003) concluded that the radio galaxies had intense, extended star-formation activity and detected on average one serendipitous source per HzRG field.

In this paper, we present James Clerk Maxwell Telescope (JCMT) SCUBA-2 (Holland et al. 2013) observations of a subset of *WISE*/radio-selected AGNs from Lonsdale et al. (submitted). The 30 luminous, dusty, high-redshift, active galaxies are selected from *WISE*, but also contain compact radio sources, in order to observe AGN feedback and potential overdense environments. They were selected on their red *WISE* mid-IR colours, with strong compact radio emission in the National Radio Astronomy Observatory (NRAO) Very Large Array (VLA) Sky Survey (NVSS; Condon et al. 1998) and/or Faint Images of the Radio Sky at Twenty cm (FIRST; Becker, White & Helfand 1995). These *WISE*/radio-selected AGNs are likely to have spectral energy distributions (SEDs) dominated by AGN that could be quenching star formation by the feedback at the highest rate of AGN fuelling, where feedback is most effective and important. The long wavelength SCUBA-2 measurements are needed to understand the cold dust properties of the target and to calculate the total IR luminosity ($L_{\rm IR}$) all the way from 8 to 1000 μm ($L_{\rm IR} = L_{8-1000\,\mu{\rm m}}$; the total IR luminosity).

Section 2 summaries the details of the sample selection from *WISE* and NVSS/FIRST data (Lonsdale et al., submitted). Section 3 describes the SCUBA-2 observations. Section 4 reports the SCUBA-2 results for SEDs and total IR luminosities ($L_{\rm IR}$), and appropriate templates in fitting the data are discussed. The maximum permitted luminosities of underlying host galaxy components are also calculated. The overdensity of serendipitous SMG sources in the SCUBA-2 fields is determined by comparison with blank-field submm surveys. The overdensity results from Hot DOGs (Jones et al. 2014) are compared, and we compared the distribution of serendipitous SMG sources within each SCUBA-2 field to HzRG fields (Stevens et al. 2003).

Throughout this paper we assume a ΛCDM cosmology with $H_0 = 71$ km s^{-1} Mpc^{-1}, $\Omega_{\rm m} = 0.27$ and $\Omega_\Lambda = 0.73$. *WISE* catalogue magnitudes are converted to flux densities using zero-point values on the Vega system of 306.7, 170.7, 29.04 and 8.284 Jy for *WISE*

3.4, 4.6, 12 and 22 μm wavelengths, respectively (Wright et al. 2010).

2 SAMPLE SELECTION

The 30 galaxies observed here with JCMT SCUBA-2 are a subset from the *WISE*/radio-selected AGNs described in more detail by Lonsdale et al. (submitted), of which 49 southern galaxies were observed with Atacama Large Millimeter/submillimeter Array (ALMA) in cycle 0. JCMT SCUBA-2 was used to observe galaxies from an independent sample in the Northern hemisphere. JCMT SCUBA-2 observations were also used to compare to the SCUBA-2 observations of Hot DOGs reported by Jones et al. (2014), and to observe the potential overdense environments surrounding the *WISE*/radio-selected AGNs.

2.1 *WISE*

WISE surveyed the entire sky at wavelengths of 3.4, 4.6, 12 and 22 μm (*W*1–*W*4) from 2010 January to 2011 January (Wright et al. 2010). One of the primary science goals was to identify the most luminous galaxies in the observable Universe, which can be accomplished due to *WISE* obtaining much greater sensitivity than previous all-sky IR survey missions. For example, *IRAS* yielded catalogued source sensitivities of 0.5 Jy at 12, 25 and 60 μm and 1 Jy at 100 μm and angular resolutions that varied from 0.5 arcmin at 12 μm to about 2 arcmin at 100 μm (Neugebauer et al. 1984), compared to *WISE* that achieved 5σ source sensitivities better than 0.054, 0.071, 0.73 and 5.0 mJy and angular resolutions of 6.1, 6.4, 6.5 and 12.0 arcsec in the *W*1–*W*4 bands, respectively (Wright et al. 2010; Jarrett et al. 2011). The objects observed here are selected from the *WISE* AllWISE Source Catalog,[1] with IR magnitudes derived using point source profile-fitting (Cutri et al. 2003).

2.2 NVSS/FIRST

NVSS is a 1.4-GHz continuum survey of the entire sky north of -40° declination, and covers 82 per cent of the sky, with an angular resolution of 45 arcsec (Condon et al. 1998). NVSS ran from 1993 to 1997 and catalogued $\sim 1.8 \times 10^6$ discrete sources with a completeness limit $\geq$2.5 mJy.

FIRST is a 1.4 GHz survey over 10 000 deg^2 of the North and South Galactic Caps at 20 cm (Becker et al. 1995). It produced 5-arcsec-resolution maps, with a typical root mean square (rms) noise level of 0.15 mJy. FIRST has a higher resolution than NVSS and so when both were available, FIRST positional data were used.

The selection criteria $0.1 < S_{22\,\mu m}/S_{1.4\,GHz} < 1$, ensures that the sample are radio-intermediate, not as radio-bright as standard radio-galaxies, 10^{40}–10^{45} erg s^{-1} (Kellermann 1974). The radio data map the synchrotron emission, and so by using this selection cut ensure that their 850 μm fluxes are not contaminated by synchrotron emission. The brightest radio source in this sample has an $S_{1.4\,GHz} = 250.2$ mJy, and most have a radio flux density between 10–100 mJy at 1.4 GHz. The weighted average $S_{1.4\,GHz} = 104.8$ mJy, and adopting a power-law spectral index of $\alpha = -1.0$, which appears to be appropriate for radio-intermediate targets (Fanti et al. 2000; Giacintucci et al. 2007; Varenius et al. 2014), the contribution to the 850 μm flux would be 0.4 mJy. When looking at the radio-loudest ($S_{1.4\,GHz} = 250.2$ mJy) and the radio-quietest ($S_{1.4\,GHz} = 12.2$ mJy) targets, the contribution to the 850 μm flux would be 1.0 and 0.04 mJy, respectively. Therefore, the sample's 850 μm fluxes, probed to a depth of 2.1 mJy beam^{-1}, should not be contaminated strongly by synchrotron emission.

The radio fluxes of the sample are similar to the luminous-infrared galaxies (LIRGs),[2] observed with the Very Long Baseline Array (VLBA) that had strong radio cores and were found to be AGN dominated (Lonsdale et al. 2003). This could imply that the strong radio emission of the *WISE*/radio-selected AGNs is evidence of significant non-thermal contributions and could be from the AGN jets. For more details see Lonsdale et al. (submitted).

The NVSS/FIRST catalogue was cross-matched with the *WISE* catalogue on <7 arcsec scales, which was best for reliability and completeness, and excluding the region within 10 deg of the Galactic plane to avoid asymptotic giant branch (AGB) stars and saturation artefacts. Matched targets with very red *WISE* colours were selected, the selection cut $(W2 - W3) + 1.25(W1 - W2) > 7$, $W4 > 10$ mJy and $W3 \geq 7$ mJy were used because coverage levels and sensitivity varies over the sky in the *WISE* survey (Lonsdale et al., submitted). The NVSS and *WISE* selection cuts were made to ensure that the targets had steep mid-IR *WISE* SEDs from *W*1–*W*4, which are consistent with AGN SEDs, with compact radio-intermediate structures. The final selection cut was for the targets to have faint or no optical counterparts to the Sloan Digital Sky Survey (SDSS) depth $r - [24] > 12.3$, to avoid confusion with bright or extended low-redshift galaxies.

These cuts led to 156 selected galaxies. The surface density of *WISE*/radio-selected high-redshift galaxies over the whole sky, to this magnitude limit, is 0.003 deg^{-2} and points to this population being exceptionally rare and perhaps an interesting transition population. They have no bright optical counterpart and are ultraluminous if at redshift $z > 0.5$. 10 targets have known redshifts, with a range $0.444 < z < 2.855$, and most of the other targets are expected to be in the same range, because they have similar *WISE* colour cuts. These redshifts ensure that the targets will benefit from the negative *K*-correction when observed at submm wavelengths.

3 OBSERVATIONS

3.1 JCMT SCUBA-2

SCUBA-2 is a submm 450/850 μm bolometer camera with eight 32 × 40 pixel detector arrays, each with a field of view of 2.4 arcmin^2. The diffraction-limited beams have full width at half maximum (FWHM) of approximately 7.5 and 14.5 arcsec, respectively (Holland et al. 2013).

From the 130 *WISE*/radio-selected AGNs, 30 that could be observed in the Northern hemisphere, were observed using SCUBA-2 on the 15-m JCMT atop Mauna Kea in Hawaii, primarily in 2013 August but also on other nights through the 12B semester, from 2012 August to 2013 January, and in the 13B semester, from 2013 August to 2014 January, and the 14A semester, from 2014 February to 2014 September. The optical depth at 225 GHz, τ_{225}, during the observations was in the range of JCMT Band 2 conditions: $0.05 < \tau_{225} < 0.08$. The corresponding opacities for each atmospheric window, 450 and 850 μm, were $0.61 < \tau_{450} < 1.18$ and

[1] http://wise2.ipac.caltech.edu/docs/release/allwise/

[2] Luminous-infrared galaxies (LIRGs), ultraluminous infrared galaxies (ULIRGs) and hyperluminous infrared galaxies (HyLIRGs) have characterizing total infrared luminosities (8–1000 μm) of $L_{8-1000\,\mu m} > 10^{11}$ L$_\odot$, $L_{8-1000\,\mu m} > 10^{12}$ L$_\odot$ and $L_{8-1000\,\mu m} > 10^{13}$ L$_\odot$, respectively (Sanders & Mirabel 1996; Lonsdale, Farrah & Smith 2006).

$0.24 < \tau_{850} < 0.40$ (Dempsey et al. 2013). Therefore, we could not use any 450 μm data because the atmospheric opacity was too great, and noise levels were too high.

All observations were taken in the 'CV Daisy observing mode that produces a 12-arcmin diameter map, with the deepest coverage in a central 3-arcmin diameter region (Holland et al. 2013). The target stays near the centre of the arrays and the telescope performs a pseudo-circular pattern with a radius of 250 arcsec at a speed of 155 arcsec s^{-1}. This mode is best for point-like sources or sources with structure smaller than 3 arcmin scales. Each scan was 25 min long and there were three scans per target, totalling an exposure time per target of 75 min.

Pointing checks were taken throughout the nights. The calibration sources observed were Uranus, CRL 2688, CRL 618 and Mars. Calibrations were taken at the start and end of every night in the standard manner (Dempsey et al. 2013).

4 RESULTS

4.1 Photometry

The maps were reduced with the Starlink SubMillimeter User Reduction Facility (SMURF) data reduction package with the 'Blank Field configuration suitable for low signal-to-noise ratio point sources (Chapin et al. 2013). SMURF performs pre-processing steps to clean the data by modelling each of the contributions to the signal from each bolometer, flat-fields the data and removes atmospheric emission and finally regrids to produce a science-quality image. Using the Starlink PIpeline for Combining and Analysing Reduced Data (PICARD) package the maps were mosaicked with all three observations per target, beam-match filtered with a 15-arcsec FWHM Gaussian and calibrated with the flux conversion factor of 2.34 Jy pW^{-1} $arcsec^{-2}$ (appropriate for aperture photometry) or 537 Jy pW^{-1} $beam^{-1}$ (in order to measure absolute peak fluxes of discrete sources) that is pertinent for 850 μm data (Dempsey et al. 2013).

The 850-μm flux densities of the 30 *WISE*/radio-selected AGNs at their *WISE* positions and the noise level in the maps are presented in Table 1, with typical rms noise of 2.1 mJy $beam^{-1}$. Four are detected at greater than 3σ significance; 21 targets had less significant positive flux measurements at the *WISE* position, with a typical significance 1.4σ; and five targets had negative flux measurements at the *WISE* position. Flux density limits were measured in an aperture diameter of 15 arcsec, the FWHM size of the telescope beam. This was an appropriate aperture size, because for the detected sources, the measured flux densities with a 15-arcsec aperture size, are consistent with the measured peak flux densities. These results can be compared to Lonsdale et al. (submitted) who observed 49 *WISE*/radio-selected AGNs in a snapshot mode with the ALMA. They detected a larger fraction of targets, with 27 out of 49 sources detected at greater than 3σ significance, in substantially deeper observations, with rms noise of 0.3–0.6 mJy. Figs 1 and 2 show the most sensitive 3-arcmin diameter SCUBA-2 850-μm DAISY fields of the four detected and four undetected *WISE*/radio-selected AGNs ordered in ascending RA, respectively. It is shown that the number of detected serendipitous SMG sources is independent of the detection of the *WISE*/radio-selected AGN target, when comparing Fig. 1 to Fig. 2. The typical offset of the *WISE* position compared with the SCUBA-2 position of the detected targets was small: 2 arcsec. Fig. 3 shows the SCUBA-2 850-μm 1.5-arcmin map of the targets W0010+1643 and W0342+3753, with contours representing 2σ and 3σ positive and negative sources.

When the images of the 26 undetected sources are stacked together into one image (Fig. 4), centred on the *WISE*-determined position of each targets, the net flux is 32.7 ± 9.0 mJy in the central 15 arcsec aperture, a detection of 3.6σ. The typical flux of an undetected target is thus likely to be approximately 1.8 mJy, which is comparable to the ALMA snapshot detection limit of Lonsdale et al. (submitted) who found a typical flux limit for an undetected target to be 1.2 mJy. The 26 undetected targets are consistent with being on average 4.5 times fainter than the four detected targets; this is consistent with Hot DOGs from Jones et al. (2014). To get deeper observations with SCUBA-2, to be able to detect more of the targets at 3σ, would require several more hours of integration per target, beyond the existing 75 mins, but would not add much more value to this stacked result, and the SCUBA-2 confusion limit is ∼1 mJy $beam^{-1}$ (Geach et al. 2013).

To test whether the positive flux density of the 26 targets with upper limits is likely to be real, 60 random points were sampled from the maps, and the stacked average flux density was 0.0 ± 0.3 mJy. This is consistent with the positive flux densities from the *WISE*/radio-selected AGNs with upper limits being due to significantly fainter, individually undetected targets.

4.2 SEDs

4.2.1 WISE-derived SEDs

The SEDs of the 10 SCUBA-2 *WISE*/radio-selected AGNs with known redshifts are shown in Fig. 5, normalized at rest-frame 3 μm and shown at rest-frame wavelengths in order to compare with various galaxy SED templates (Polletta et al. 2007) in order to illustrate the nature of the *WISE*/radio-selected AGNs. The mid-IR SEDs of the 20 *WISE*/radio-selected AGNs with unknown redshifts are shown in Fig. 6, with the Polletta SED templates redshifted to $z = 2$. The Polletta galaxy templates are Arp 220 (starburst-dominated galaxy), Mrk 231 (heavily obscured AGN-starburst composite), quasar (QSO) 1 and 2 (optically selected QSOs of types 1 and 2), spiral (Spiral Sb), torus (type-2 heavily obscured QSO, that is believed to be an accreting SMBH with a hot accretion disc surrounded by dust and Compton-thick gas in a toroidal structure; Krolik & Begelman 1988). The SEDs are broadly similar at mid-IR wavelengths. They have a steep red power-law IR (1–5 μm) section, and a potential mid-IR peak from hot dust emission that is bluewards of the AGN SED templates, turning over to a Rayleigh–Jeans spectrum longwards of 200 μm due to the coolest dust emission. The SEDs are not well-represented by any of the Polletta templates; the closest fitting template is the single Polletta torus template. The SEDs are consistent with those of the 49 ALMA observed *WISE*/radio-selected AGNs (Lonsdale et al., submitted). All *WISE*/radio-selected AGNs have hotter *WISE*/submm colours than standard pre-existing AGN template SEDs.

The Hot DOGs (Wu et al. 2012; Jones et al. 2014) have broadly similar SED shapes compared to the *WISE*/radio-selected AGNs here and from Lonsdale et al. (submitted): they all have bluer mid-IR sections and turn over into the submm at shorter wavelengths than typical SED templates. However, the Hot DOGs have steeper mid-IR sections that could be because these galaxies have redder *WISE* colour selection cuts and a greater average redshift, for example the average redshift in this paper is $z = 1.3$, and in Lonsdale et al. (submitted) the average redshift is $z = 1.7$, whereas the average redshift in Jones et al. (2014) was higher at $z = 2.7$. The *WISE* colours for the *WISE*/radio-selected AGNs are $(W1 - W2) = 1.80$ and $(W2 - W3) = 4.80$, compared with Hot DOGs, $(W1 - W2) = 1.77$

Table 1. Coordinates and photometry of the 30 WISE/radio-selected AGNs, with 3.4, 4.6, 12 and 22 μm magnitudes from AllWISE Source Catalog and 850-μm flux densities from SCUBA-2. The top four targets are detected at 850 μm, while the bottom 26 targets have upper limits at 850 μm. For redshifts refer Lonsdale et al. (submitted). The submm to mid-IR ratios for undetected SCUBA-2 targets are calculated using the 2σ SCUBA-2 limit.

Source	RA (J2000)	Dec. (J2000)	3.4 μm (mag)	4.6 μm (mag)	12 μm (mag)	22 μm (mag)	850 μm (mJy)	850 μm/22 μm Ratio	NVSS 1.4 GHz (mJy beam^{-1})	FIRST 21 cm (mJy)	Redshift
W0849+3033	08:49:04.16	+30:33:37.0	16.78 ± 0.09	15.73 ± 0.17	10.04 ± 0.07	6.99 ± 0.10	9.0 ± 2.4	0.7 ± 0.2	16.1 ± 0.6	15.69 ± 0.14	Unknown
W2212+3326	22:12:58.80	+33:26:04.9	15.62 ± 0.04	13.50 ± 0.03	9.49 ± 0.04	7.20 ± 0.12	7.8 ± 2.0	0.7 ± 0.2	45.8 ± 1.4	No coverage	Unknown
W2331−1411	23:31:03.17	−14:11:52.2	16.72 ± 0.11	15.41 ± 0.11	9.90 ± 0.06	7.02 ± 0.09	8.8 ± 2.2	0.7 ± 0.2	134.8 ± 4.1	No coverage	Unknown
W2345+3120	23:45:41.23	+31:20:25.8	16.56 ± 0.07	15.16 ± 0.08	10.09 ± 0.06	6.94 ± 0.11	6.7 ± 2.0	0.5 ± 0.2	15.0 ± 0.6	No coverage	Unknown
W0010+1643	00:10:39.50	+16:43:28.7	17.74 ± 0.22	15.94 ± 0.17	10.26 ± 0.08	7.19 ± 0.09	3.8 ± 1.9	< 0.7	18.5 ± 0.7	No coverage	2.855
W0244+1123	02:44:23.99	+11:23:54.4	14.99 ± 0.03	12.65 ± 0.03	8.40 ± 0.02	6.30 ± 0.05	3.0 ± 2.1	< 0.3	37.7 ± 1.2	No coverage	Unknown
W0332+3205	03:32:28.23	+32:05:45.0	15.86 ± 0.08	14.57 ± 0.06	9.79 ± 0.06	6.50 ± 0.07	−2.2 ± 2.0	< 0.1	42.1 ± 1.3	No coverage	Unknown
W0342+3753	03:42:22.94	+37:53:30.7	15.13 ± 0.04	14.42 ± 0.05	9.39 ± 0.04	6.32 ± 0.06	0.3 ± 2.1	< 0.2	154.5 ± 5.5	No coverage	0.47
W0352+1947	03:52:05.35	+19:47:01.2	16.65 ± 0.10	14.58 ± 0.06	9.74 ± 0.05	7.39 ± 0.13	1.0 ± 2.1	< 0.6	17.7 ± 0.7	No coverage	Unknown
W0404+0712	04:04:40.93	+07:12:19.2	16.64 ± 0.09	15.06 ± 0.08	10.02 ± 0.05	7.14 ± 0.09	2.3 ± 1.9	<0.2	189.5 ± 5.7	No coverage	Unknown
W0443+0643	04:43:32.56	+06:43:18.1	16.57 ± 0.09	14.91 ± 0.09	9.38 ± 0.05	7.13 ± 0.14	6.8 ± 3.7	< 0.6	17.9 ± 0.7	No coverage	Unknown
W1025+6128	10:25:09.87	+61:28:32.7	16.03 ± 0.05	13.66 ± 0.03	8.19 ± 0.02	5.74 ± 0.04	2.7 ± 2.0	< 0.1	60.2 ± 2.2	30.68 ± 0.14	Unknown
W1046−0250	10:46:32.81	−02:50:30.7	16.55 ± 0.09	14.48 ± 0.06	10.07 ± 0.07	7.07 ± 0.10	−0.4 ± 2.1	< 0.3	79.1 ± 2.4	85.10 ± 0.13	Unknown
W1107+3421	11:07:34.34	+34:21:18.7	15.02 ± 0.03	12.79 ± 0.03	8.93 ± 0.03	7.01 ± 0.09	2.2 ± 2.0	< 0.5	22.3 ± 0.8	20.56 ± 0.13	Unknown
W1210+4750	12:10:27.88	+47:50:03.2	16.91 ± 0.09	14.96 ± 0.07	9.66 ± 0.04	7.08 ± 0.09	3.4 ± 2.3	< 0.7	23.7 ± 0.1	26.1 ± 0.9	Unknown
W1212+4659	12:12:04.91	+46:59:58.9	16.07 ± 0.05	13.92 ± 0.04	9.61 ± 0.04	7.26 ± 0.11	3.3 ± 2.5	< 0.8	21.2 ± 0.7	21.69 ± 0.15	Unknown
W1409+1732	14:09:28.83	+17:32:04.3	17.39 ± 0.13	16.06 ± 0.14	10.07 ± 0.05	7.05 ± 0.08	5.2 ± 2.0	< 0.7	14.8 ± 0.6	21.49 ± 0.27	Unknown
W1428+1113	14:28:59.69	+11:13:18.7	16.68 ± 0.07	15.22 ± 0.07	9.63 ± 0.04	7.21 ± 0.08	2.2 ± 2.2	< 0.6	12.2 ± 0.5	9.92 ± 0.15	1.6
W1501+1324	15:01:38.36	+13:24:49.9	14.33 ± 0.03	12.14 ± 0.02	8.18 ± 0.02	6.55 ± 0.05	−2.8 ± 2.2	< 0.1	250.2 ± 7.5	254.44 ± 0.14	0.505
W1517+3523	15:17:58.61	+35:23:54.3	15.66 ± 0.04	13.47 ± 0.03	9.03 ± 0.03	6.51 ± 0.05	−0.9 ± 1.9	< 0.1	41.0 ± 1.3	42.14 ± 0.15	1.515
W1630+5126	16:30:36.23	+51:26:12.7	15.56 ± 0.05	14.11 ± 0.03	9.58 ± 0.03	7.06 ± 0.06	1.7 ± 1.9	< 0.4	105.4 ± 3.2	100.81 ± 0.14	Unknown
W1703+2615	17:03:34.21	+26:15:11.1	15.45 ± 0.04	13.65 ± 0.03	9.00 ± 0.03	6.95 ± 0.08	3.2 ± 2.0	< 0.5	56.0 ± 1.7	58.64 ± 0.15	Unknown
W1717+5313	17:17:05.92	+53:13:42.6	15.49 ± 0.05	13.70 ± 0.03	9.49 ± 0.03	7.19 ± 0.07	3.5 ± 2.5	< 0.8	20.2 ± 0.7	13.82 ± 0.14	2.717
W2126−0103	21:26:19.97	−01:03:54.3	15.01 ± 0.04	13.17 ± 0.03	8.84 ± 0.03	7.29 ± 0.13	1.8 ± 2.0	< 0.6	12.9 ± 0.9	No coverage	0.607
W2133−1419	21:33:56.51	−14:19:04.6	15.88 ± 0.06	14.12 ± 0.05	9.65 ± 0.05	6.85 ± 0.09	1.6 ± 1.8	< 0.4	22.3 ± 1.1	No coverage	Unknown
W2212−1253	22:12:05.05	−12:53:47.0	15.60 ± 0.05	14.51 ± 0.06	9.55 ± 0.05	6.89 ± 0.10	−0.1 ± 2.1	< 0.3	125.7 ± 4.4	No coverage	Unknown
W2222+0951	22:22:48.76	+09:51:29.2	15.79 ± 0.05	13.97 ± 0.04	9.67 ± 0.04	7.16 ± 0.11	3.1 ± 2.0	< 0.6	17.1 ± 0.7	No coverage	Unknown
W2226+0025	22:26:25.12	+00:25:09.6	15.81 ± 0.05	14.40 ± 0.05	9.50 ± 0.05	7.07 ± 0.11	3.4 ± 1.9	< 0.6	17.0 ± 1.0	15.76 ± 0.10	0.676
W2230−0720	22:30:07.75	−07:20:59.9	15.49 ± 0.04	13.67 ± 0.04	9.26 ± 0.04	6.95 ± 0.10	1.4 ± 1.8	< 0.4	46.4 ± 1.5	No coverage	0.444
W2325−0429	23:25:05.07	−04:29:48.1	15.88 ± 0.05	14.49 ± 0.06	9.65 ± 0.05	7.11 ± 0.10	2.9 ± 2.1	< 0.6	149.8 ± 4.5	No coverage	1.737

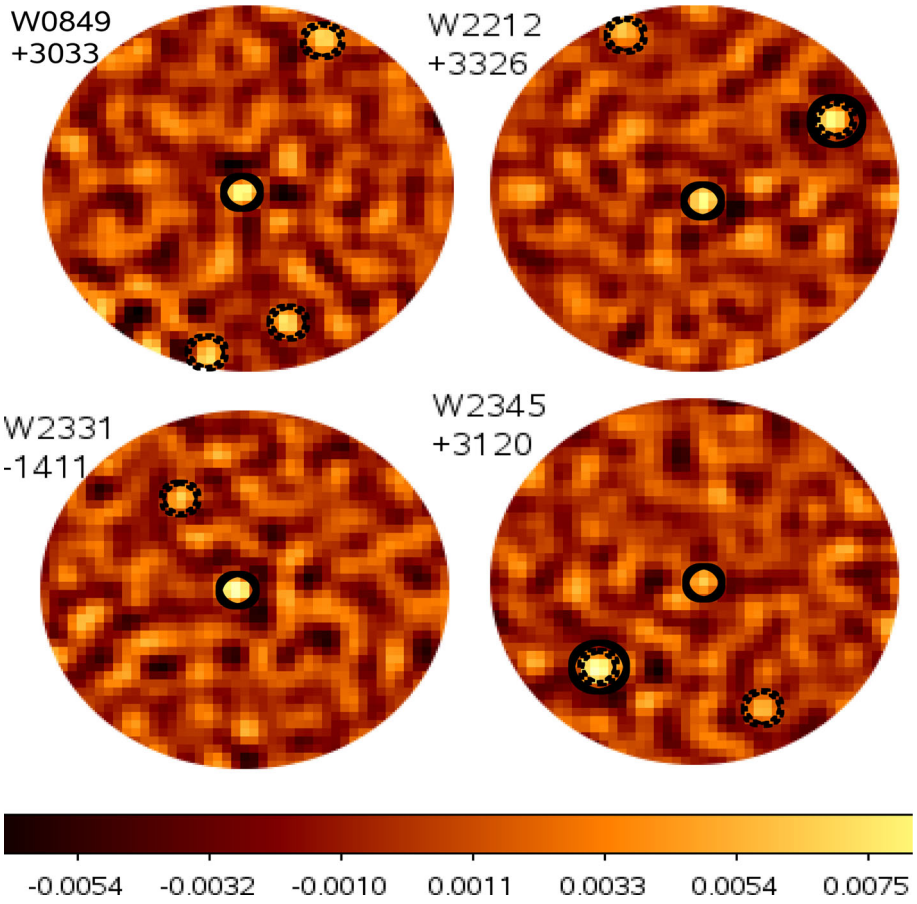

Figure 1. SCUBA-2 850-μm 1.5-arcmin radius maps of the four detected targets: W0849+3033, W2212+3326, W2331−1411 and W2345+3120. The solid circles show the 15-arcsec beam-sized apertures centred on the *WISE* positions of the targets. Serendipitous sources brighter than 3σ and within 1.5 arcmin of the *WISE* target are shown by the dotted 15-arcsec beam-sized circles, and serendipitous sources brighter than 4σ are shown by a dotted 15-arcsec beam-sized circle surrounded by a solid black circle. It is shown that the number of detected serendipitous SMG sources is independent of the detection of the *WISE*/radio-selected AGN target, when compared to Fig. 2. The colour flux bar at the bottom is in Jy. North is up, east is to the left.

and $(W2 - W3) = 6.13$. When *K*-correcting the Hot DOG *WISE* colours to *WISE*/radio-selected AGN redshifts, the *WISE* colours expected are $(W1 - W2) = 3.56$ and $(W2 - W3) = 6.38$. The *WISE* colours show that the Hot DOGs appear to be mid-IR redder, and could be due to the sources having more obscuration than the WISE/radio-selected AGNs, which can be seen in the SEDs in Fig. 5 when compared to the SEDs in fig. 5 from Jones et al. (2014). Alternatively, it could be because the Hot DOGs are typically at a higher redshift, and were selected to be mid-IR redder.

4.2.2 SCUBA-2-derived SEDs

Normalized to the *WISE* data at rest frame 3 μm that lies within the *WISE* rest-frame wavelength range for all of our targets, the SCUBA-2 data in the normalized SED show that the detected *WISE*/radio-selected AGNs have less submm emission than the Polletta torus template, with an average submm flux three times less than the template; Fig. 5. Most of the undetected *WISE*/radio-selected AGNs have limits that demand their submm emission to be less than the Polletta torus template, with a flux difference factor range of 1–9. Less submm emission is also seen in the SEDs of Hot DOGs (Wu et al. 2012; Jones et al. 2014). This leads to the suggestion that the *WISE*/radio-selected AGNs have less cold dust in the host galaxy and/or on the outer edge of the torus, and hence the torus could be denser and smaller than assumed in the template. Alternatively, less submm emission could be due to excess mid-IR emission from AGN heating relative to the torus template (Wu et al. 2012). The 22-μm (*W*4) flux densities and the 850-μm flux densities of the 30 *WISE*/radio-selected AGNs and the 10 Hot DOGs are comparable, as shown in Fig. 7: the serendipitous SMG sources detected around the *WISE*/radio-selected AGNs that have *WISE* data are also plotted in blue and will be discussed in Section 6.2. The Hot DOGs in Jones et al. (2014) are submm brighter, because 60 per cent Hot DOGs are submm detected compared to 13 per cent *WISE*/radio-selected AGNs; the average submm flux of detected Hot DOGs was 8.3 ± 1.8 mJy, which is similar to the average submm flux of detected *WISE*/radio-selected AGNs, 8.1 ± 2.2 mJy. However, the Hot DOGs are typically at $z \sim 2.7$, compared to $z \sim 1.7$ for the *WISE*/radio-selected AGNs. Considering that when *K*-correcting the *WISE*/radio-selected AGNs 850-μm flux density to the Hot DOG redshift, it should be $S_{850\,\mu\mathrm{m}}$ 16 ± 3 mJy, indicating the *WISE*/radio-selected AGNs are submm fainter than the Hot DOGs. However, this is only an estimate because there are only a small number (10) known redshifts.

To investigate if the SEDs are dominated by warm or cool dust the submm to mid-IR ratios ($F_{850\,\mu\mathrm{m}}/F_{22\,\mu\mathrm{m}}$) of the 30 targets in the observed frame are listed in Table 1; for undetected targets, the 850-μm 2σ upper limits are reported. The weighted average $F_{850\,\mu\mathrm{m}}/F_{22\,\mu\mathrm{m}}$ of the four detected targets is 0.7 ± 0.2, where

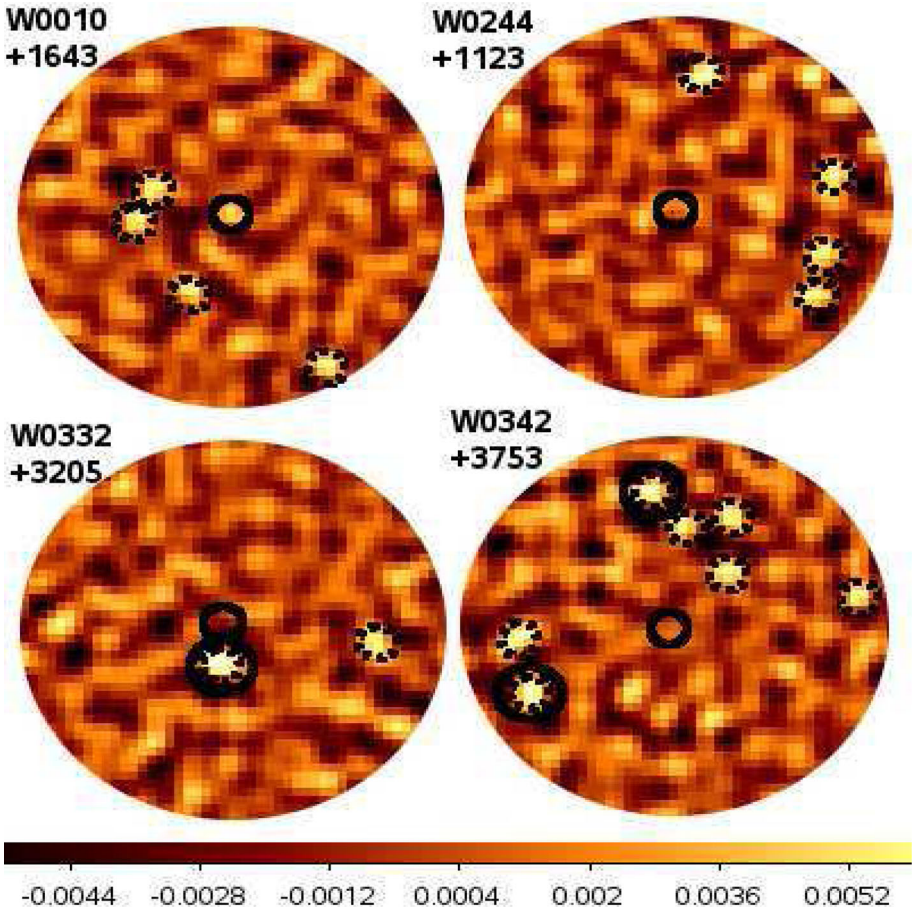

Figure 2. SCUBA-2 850-μm 1.5-arcmin radius maps of a sample of four undetected targets ordered by RA Dec.: W0010+1643, W0244+1123, W0332+3205 and W0342+3753. The solid circles show the 15-arcsec beam-sized apertures centred on the *WISE* positions of the targets. Serendipitous sources brighter than 3σ and within 1.5 arcmin of the *WISE* target are shown by the dotted 15-arcsec beam-sized circles, and serendipitous sources brighter than 4σ are shown by the dotted 15-arcsec beam-sized circle surrounded by a solid black circle. It is shown that the number of detected serendipitous SMG sources is independent of the detection of the *WISE*/radio-selected AGN target, when compared to Fig. 1. The colour flux bar at the bottom is in Jy. North is up, east is to the left.

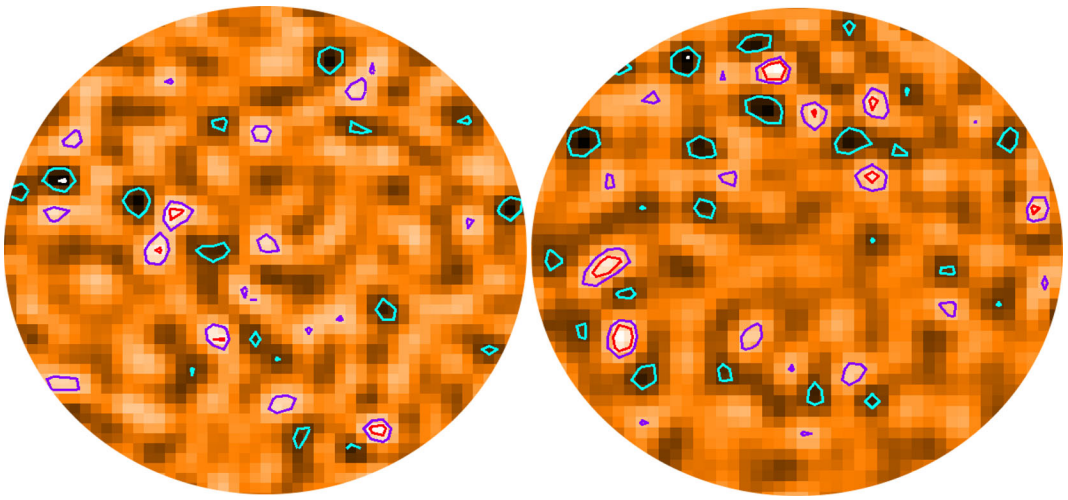

Figure 3. SCUBA-2 850-μm 1.5-arcmin radius maps showing the central region of the first target when ordered by RA Dec. W0010+1643 and the field with the largest number of detected serendipitous SMG sources (7) W0342+3753, with flux density contours: white represents negative 3σ, blue represents negative 2σ, purple represents positive 2σ and red represents positive 3σ. North is up, east is to the left.

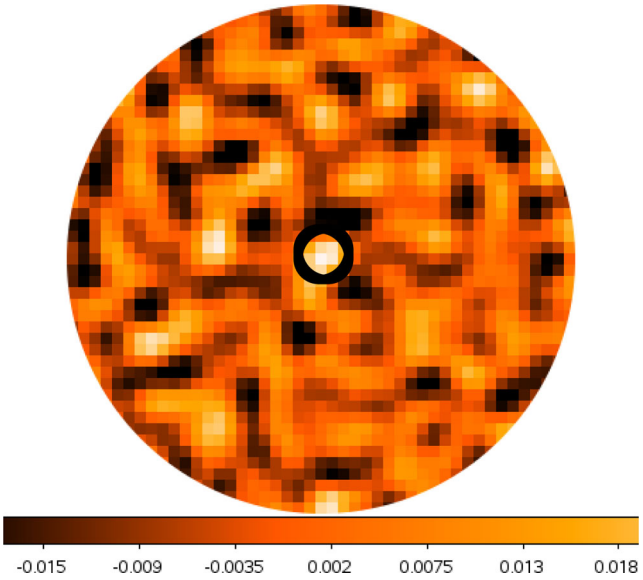

Figure 4. SCUBA-2 850-μm 1.5-arcmin radius map showing the central regions of the maps of the 26 undetected targets stacked together. The circle shows the central 15 arcsec area. The colour flux bar at the bottom is in Jy. North is up, east is to the left.

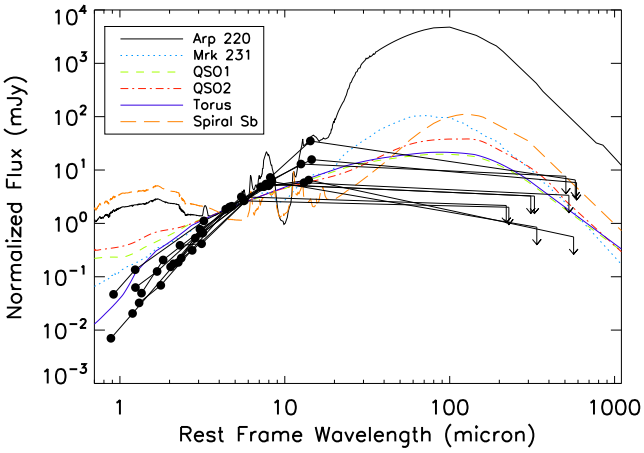

Figure 5. SEDs of the 10 *WISE*/radio-selected AGNs with known redshifts, including the 850-μm SCUBA-2 data in rest-frame wavelengths with Arp 220, Mrk 231, QSO 1, QSO 2, Torus and Spiral Sb galaxy templates from Polletta et al. (2007), normalized at rest frame 3 μm. Detections are represented by filled circles, while 2σ upper limits are represented by arrows. The data points for the *WISE*/radio-selected AGNs are connected for clarity, and do not represent the true SED. The 10 *WISE*/radio-selected AGNs are not well-fitted by the standard AGN templates, with extra dust extinction required, which is consistent with Hot DOGs (Jones et al. 2014).

the error is the weighted standard error. This is consistent with the weighted average $F_{850\,\mu m}/F_{22\,\mu m} = 0.6 \pm 0.1$ of Hot DOGs (Jones et al. 2014). Fig. 8 shows these ratios in the observed sample and for the Polletta AGN torus templates as a function of redshift. Most of the targets have a lower submm to mid-IR flux ratio than the torus template (Fig. 8), but show no sign of an expected *K*-correction with redshift as expected from the template SEDs: in particular the five highest redshift *WISE*/radio-selected AGNs have submm emission that lies beneath the torus template, and similar observed submm to mid-IR ratios to the lower redshift *WISE*/radio-selected AGNs. They also have the most luminous luminosities dominated by the

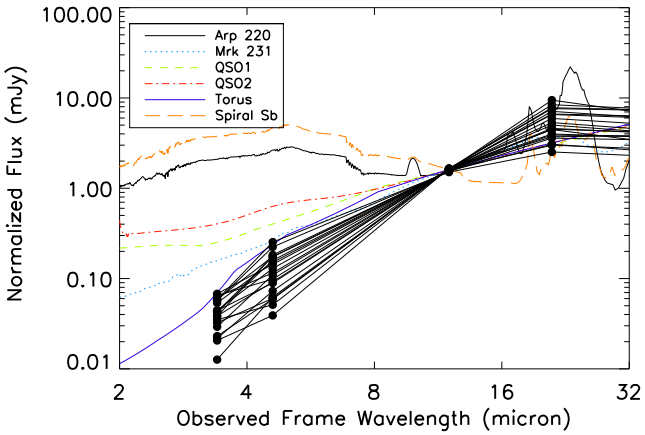

Figure 6. Mid-IR SEDs of the 20 *WISE*/radio-selected AGNs showing the range of *WISE* data, in observed-frame wavelengths Arp 220, Mrk 231, QSO 1, QSO 2, Torus and Spiral Sb galaxy templates (Polletta et al. 2007) redshifted to $z = 2$ and normalized at observed frame 12 μm. Detections are represented by filled circles, while 2σ upper limits are represented by arrows. The data points for the *WISE*/radio-selected AGNs are connected for clarity, and do not represent the true SED.

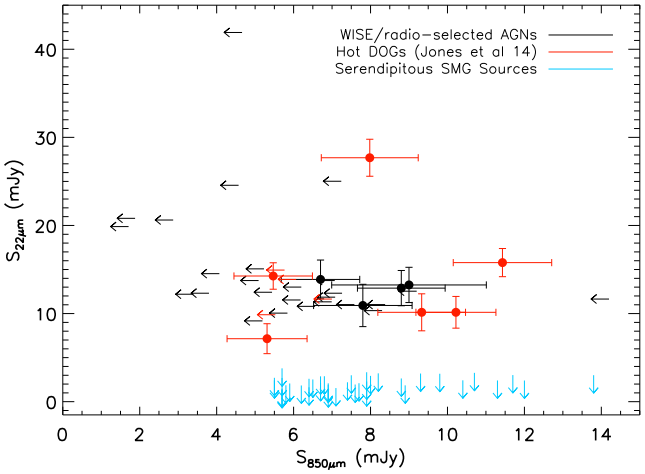

Figure 7. The *W*4 (22-μm) flux density versus 850-μm flux density for the 30 *WISE*/radio-selected AGNs in black, the 10 Hot DOGs in red (Jones et al. 2014) and the 39 serendipitous SMG sources detected around the *WISE*/radio-selected AGNs that have *WISE* data in blue. Detections are represented by filled circles, while 2σ upper limits are represented by arrows.

mid-IR emission, which could suggest that they have hotter effective dust temperatures compared with the rest of the sample. This is in agreement with the results from submm observations of Hot DOGs (Wu et al. 2012; Jones et al. 2014), and suggest that Hot DOGs and *WISE*/radio-selected AGNs are both dominated by warm dust, with lower $F_{850\,\mu m}/F_{22\,\mu m}$ than standard torus SED templates.

4.3 Luminosities

A conservative lower limit to the total IR luminosities of the galaxies was estimated by connecting all the *WISE* and SCUBA-2 data points with power laws and then integrating, without extrapolating beyond the range of the data in wavelength, ($L_{8\,\mu m-SCUBA2}$), the targets without redshift have assumed redshifts of $z = 2.0$. This luminosity

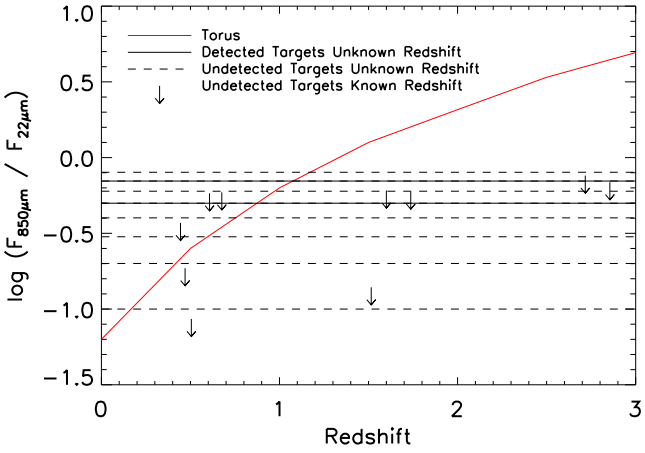

Figure 8. The submm to mid-IR ratio ($F_{850\,\mu m}/F_{22\,\mu m}$) of the 10 targets with known redshifts. The detected targets with unknown redshifts have solid lines, and the undetected targets have dashed lines across the redshift range $0.3 \leq z \leq 3$. The red solid line represents the Polletta torus template (Polletta et al. 2007) as a function of redshift, and 2σ upper limits are represented by arrows.

is a very conservative estimate because any strong peak in the SED would not be included in the power-law interpolation, and it spans a minimal wavelength range. The resulting $L_{8\,\mu m-SCUBA2}$ values for the 30 *WISE*/radio-selected AGNs are presented in Table 2. The four detected targets have a range from $(1.7 \pm 2.5) \times 10^{13}$ to $(6.2 \pm 1.7) \times 10^{13}$ $L_\odot$, if their redshifts are all consistent with the subset of 10 targets with known redshifts $z \sim 0.4$–2.9, using $z = 2$. This classifies them as HyLIRGs (see footnote 2).

We also use the SCUBA-2 data to limit the luminosity of an underlying extended host galaxy not associated with the *WISE*/radio-selected AGN, powered by star-forming activity. A spiral (Sb) galaxy SED template and a warmer ULIRG/starburst-type (Arp 220) SED template were normalized to account for all of the SCUBA-2 850-μm flux density, and then the maximum total luminosity of these components of the SED were estimated by integrating under the Sb or Arp 220 template. This approach assumes that an underlying extended dusty galaxy, disconnected from the mid-IR emission of the AGN, accounts for all of the measured SCUBA-2 flux. It is assumed to be solely due to star formation rather than an AGN. An Sb host galaxy template cannot exceed ∼4 per cent of the inferred *WISE*/radio-selected AGN luminosity from the four detected targets. This would give a Sb luminosity of 4.9×10^{12} $L_\odot$, 80 times more luminous than the Milky Way, with an equivalent star formation rate (SFR) of ∼110 $M_\odot$ yr^{-1}. An Arp 220 ULIRG template that accounts for all the 850 μm flux has a luminosity of 1.1×10^{13} $L_\odot$, ∼10 per cent of the inferred *WISE*/radio-selected AGN luminosity from the four detected targets, with an equivalent SFR of ∼250 $M_\odot$ yr^{-1}. This emphasizes that the full *WISE*/radio-selected AGN SED from 8–1000 μm has a small contribution from cold far-IR dust traced by the SCUBA-2 observations, and is dominated by hot dust and mid-IR emission from the AGN. This is consistent with the results from SCUBA-2 observations of Hot DOGs, which found that an underlying Sb-type galaxy SED template contributes less than 2 per cent to the typical total Hot DOG IR luminosity; however, an Arp 220-type galaxy SED template contributes less than 55 per cent, this is because the Hot DOGs are submm brighter and could suggest there is more star-formation activity in Hot DOGs compared to *WISE*/radio-selected AGNs.

Table 2. The total IR luminosities (8 μm − SCUBA2) of the 30 WISE/radio-selected AGNs derived by connecting all the WISE and SCUBA-2 data points with power laws and then integrating. The top four have detections at 850 μm and the bottom 26 have 2σ upper limits at 850 μm. The targets without redshift data, have assumed redshifts of $z = 2$. The luminosities are shown in solar luminosities, 3.84×10^{26} W.

Source	Total IR luminosities (8 μm − SCUBA2) ($L_\odot$)
W0849+3033	$1.7 \pm 2.5 \times 10^{13}$
W2212+3326	$6.2 \pm 1.7 \times 10^{13}$
W2331−1411	$1.8 \pm 1.8 \times 10^{13}$
W2345+3120	$1.7 \pm 2.6 \times 10^{13}$
W0010+1643	$<3.4 \times 10^{13}$
W0244+1123	$<3.7 \times 10^{13}$
W0332+3205	$<2.0 \times 10^{13}$
W0342+3753	$<7.5 \times 10^{11}$
W0352+1947	$<1.4 \times 10^{13}$
W0404+0712	$<1.5 \times 10^{13}$
W0443+0643	$<2.9 \times 10^{13}$
W1025+6128	$<5.1 \times 10^{13}$
W1046−0250	$<1.4 \times 10^{13}$
W1107+3421	$<2.2 \times 10^{13}$
W1210+4750	$<1.5 \times 10^{13}$
W1212+4659	$<1.7 \times 10^{13}$
W1409+1732	$<1.7 \times 10^{13}$
W1428+1113	$<9.3 \times 10^{12}$
W1501+1324	$<1.2 \times 10^{12}$
W1517+3523	$<1.3 \times 10^{13}$
W1630+5126	$<1.7 \times 10^{13}$
W1703+2615	$<2.2 \times 10^{13}$
W1717+5313	$<3.8 \times 10^{13}$
W2126−0103	$<1.1 \times 10^{12}$
W2133−1419	$<1.8 \times 10^{13}$
W2212−1253	$<1.8 \times 10^{13}$
W2222+0951	$<1.6 \times 10^{13}$
W2226+0025	$<1.2 \times 10^{12}$
W2230−0720	$<4.9 \times 10^{11}$
W2325−0429	$<1.2 \times 10^{13}$

5 ENVIRONMENTS AROUND *WISE*/RADIO-SELECTED AGNS

Serendipitous SMG sources are detected in the deepest SCUBA-2 1.5-arcmin-radius regions around the *WISE*/radio-selected AGNs. To investigate if there is an overdensity of SMGs in the *WISE*/radio-selected AGN fields, the serendipitous source number counts are compared with those in two different blank-field submm surveys, in a similar method to Jones et al. (2014). To provide another test, 1.5-arcmin-radius circles were placed at random in a blank-field submm survey and the number of galaxies counted, again in a similar method to Jones et al. (2014). The differential number counts are then measured and compared to three different blank-field submm surveys.

81 serendipitous 850 μm sources were detected at greater than 3σ in the 30 SCUBA-2 maps, and 11 sources were detected at greater than 4σ; see Table 3. The total area surveyed was 212 $arcmin^2$, or about 4000 SCUBA-2 850 μm beams. There are 8±3 negative peaks in the 30 maps above the same 3σ threshold (see Table 3), consistent with the six 3σ negative peaks expected from Gaussian noise, with width of the SCUBA-2 FWHM beam (14 arcsec).

To see if there is evidence for an overdensity of SMGs in the 30 *WISE*/radio-selected AGNs fields, the number of serendipitous

Table 3. Number of serendipitous sources counted in each of the 30 maps at greater than 3σ and 4σ significance, and the number of negative peaks at greater than 3σ significance. There were no negative peaks at greater than 4σ significance.

Source	Number of serendipitous sources at greater than 3σ	Number of serendipitous sources at greater than 4σ	Number of negative peaks at greater than 3σ
W0010+1643	4	0	1
W0244+1123	4	0	0
W0332+3205	2	1	0
W0342+3753	7	2	1
W0352+1947	1	0	1
W0404+0712	2	0	0
W0443+0643	3	0	0
W0849+3033	3	0	0
W1025+6128	3	0	0
W1046−0250	3	0	1
W1107+3421	2	0	0
W1210+4750	5	1	0
W1212+4659	3	0	0
W1409+1732	3	0	0
W1428+1113	1	0	0
W1501+1324	4	0	1
W1517+3523	5	0	0
W1630+5126	2	0	0
W1703+2615	1	0	0
W1717+5313	3	1	0
W2126−0103	1	0	0
W2133−1419	1	0	1
W2212−1253	2	0	0
W2212+3326	2	1	0
W2222+0951	3	2	0
W2226+0025	2	1	0
W2230−0720	4	0	1
W2325−0429	2	1	1
W2331−1411	1	0	0
W2345+3120	2	1	0

sources can be compared with the results of blank-field submm surveys. In the LABOCA ECDFS Submm Survey (LESS) survey, Weiß et al. (2009) detected 126 SMGs in a uniform area of 1260 arcmin^2 surveyed with a noise level of 1.2 mJy at 870 μm. They found evidence for an angular clustering signal on scales of 1 arcmin. There are 60 LESS sources brighter than our average 3σ flux density limit of 6.2 mJy. If the average surface number density of SMGs holds in our SCUBA2 maps, so no cosmic variance between the fields, 10.1 serendipitous sources would be expected within 1.5 arcmin of our 30 targeted fields; however, we have identified 64. This indicates a relative overdensity of SMGs in our *WISE*/radio-selected AGN fields by a factor of 6.3 ± 1.1.

The average noise level of our maps is 2.1 beam^{-1}, slightly higher than the average noise level of the deeper observations of Hot DOGs 1.8 mJy beam^{-1} reported in Jones et al. (2014).

In order to check the effect of our range of sensitivity in each field we also compare the number of SMGs at our average 4σ noise level with the LESS survey. The number of LESS sources brighter than our average 4σ flux density limit of 8.2 mJy is 23 SMGs, which suggests that 3.9 serendipitous sources would be expected in our 30 SCUBA-2 fields. We identified 19 and thus a relative overdensity of SMGs by a factor of 4.9 ± 1.5. The overdensity above the average 3σ noise level is consistent with that above the average 4σ noise level; therefore, the ∼30 per cent range in the 30 map noise levels is unlikely to have a large effect on the overdensity factor.

A complementary way to test whether there is an overdensity of SMGs near the *WISE*/radio-selected AGN targets is to place 1.5-arcmin-radius SCUBA-2 field circles at random locations in the LESS field and count the number of sources from the catalogue source positions that would have been detected in our survey, taking into account the differences in depth, by employing our average 3σ flux density limit of 6.2 mJy. In 100 randomly selected 1.5-arcmin-radius circles within LESS, we found 32 ± 3 LESS sources brighter than 6.2 mJy; the error is estimated from repeating this process three times. The total number of 1.5-arcmin-radius fields within LESS is ∼200. Thus, in the 30 *WISE*/radio-selected AGN maps we would expect 10.1 serendipitous sources based on LESS taking into account our field depths; however, we find 64. There is thus a relative overdensity of SMGs around *WISE*/radio-selected AGNs by a consistent factor of 6.3 ± 1.4 as compared with this blank field.

In 100 randomly selected 1.5-arcmin-radius circles within LESS, we found 13 ± 2 LESS sources brighter than the 8.2 mJy average 4σ noise level. From this it can be predicted that in the 30 *WISE*/radio-selected AGN maps there should be 3.9 serendipitous sources; however, we find 19. Thus the relative overdensity of 4σ SMGs around *WISE*/radio-selected AGNs is by a factor of 4.9 ± 1.8 as compared with this blank field. Again the overdensity using the average 3σ noise level is consistent with that using the average 4σ noise level; therefore, the difference in the 30 map noise levels appears not to have a large effect on the overdensity factor.

The overdensity factor of SMGs from the *WISE*/radio-selected AGN fields to the LESS field ranges from 4.9–6.3, with a weighted average of 5.3. Weiß et al. (2009) conclude that in the LESS field there is a cumulative source count lower by a factor ∼2 compared with another deep submm survey, the SCUBA Half-Degree Extragalactic Survey (SHADES; Coppin et al. 2006). This implies that our *WISE*/radio-selected AGN fields could have an overdensity that is tripled compared with other previous submm surveys.

Fig. 9 compares the differential number counts for all 30 *WISE*/radio-selected AGN SCUBA-2 fields compared to previous blank-field submm surveys, including LESS and SHADES, and all 10 Hot DOG SCUBA-2 maps (Jones et al. 2014). It is seen that

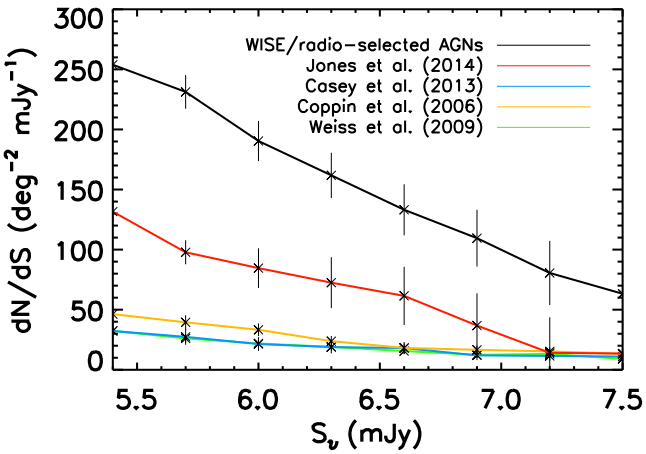

Figure 9. The differential number counts for all 30 *WISE*/radio-selected AGN SCUBA-2 maps, compared with 10 Hot DOG SCUBA-2 maps (Jones et al. 2014), the LESS survey (Weiß et al. 2009), the COSMOS survey (Casey et al. 2013) and SHADES (Coppin et al. 2006).

the fields around *WISE*/radio-selected AGNs are overdense compared with other submm surveys, and Hot DOGs are also overdense compared with other submm surveys, which is consistent with the results above. The *WISE*/radio-selected AGNs are at high Galactic latitudes, and therefore there is less possibility for the high surface number density to be just foreground contamination.

We repeat this approach in another submm blank-field survey. Casey et al. (2013) used SCUBA-2 to observe the Cosmological Evolution Survey (COSMOS) field over a uniform area of 394 arcmin^2 to a noise level of 0.80 mJy at 850 μm and detected 99 SMGs brighter than 3.6σ. There are 21 COSMOS sources brighter than our average detection threshold of 6.2 mJy (3σ), which would imply 11.3 serendipitous sources expected in the 30 SCUBA-2 *WISE*/radio-selected AGN fields. We find 64, implying a relative overdensity of SMGs by a factor of 5.7 ± 1.4, consistent with 6.3 ± 1.1 from LESS. Nine COSMOS sources are brighter than our 4σ flux density limit of 8.2 mJy, which implies that 4.8 4σ serendipitous sources would be expected in our 30 SCUBA-2 fields. However, we find 19 and thus a relative overdensity of SMGs by a factor of 4.0 ± 1.6, consistent with 4.9 ± 1.5 from LESS. Again, the variation in noise levels of the 30 *WISE*/radio-selected AGN field does not appear to have a large effect on the overdensity factor. Random 1.5-arcmin-radius circles were not placed in the smaller COSMOS field as only ∼50 1.5-arcmin-radius fields are available. The COSMOS field is noisier at the edge of the map due to the JCMT PONG observing mode, and the noise level could be double at the edge of their 850 μm map. Therefore, to detect a source brighter than their 3.6σ limit, the source would need a flux density of greater than 5.8 mJy. This could be a problem because our source detection limit is lower at 3σ and sources could be missed. However, it will not affect our overdensity results because our 3σ average detection threshold is greater (6.2 mJy) than their noisiest 3.6σ limit (5.8mJy), and thus no COSMOS sources would be missed when comparing number counts from their catalogue.

17 serendipitous sources were found in the 10 SCUBA-2 fields of Hot DOGs reported by Jones et al. (2014), who concluded that these fields had an SMG overdensity by factor of ∼2–3 compared with the LESS and COSMOS fields. At our average 3σ flux density of 6.2 mJy, there were 9 serendipitous sources found in the 10 SCUBA-2 Hot DOGs, which would imply 26.9 serendipitous sources are expected in these 30 SCUBA-2 *WISE*/radio-selected AGNs. However, we find 64 and suggest that the *WISE*/radio-selected AGN fields have a higher density of SMGs than the Hot DOGs by a factor of 2.4 ± 0.9, and have an even higher overdensity compared with the LESS and COSMOS fields than the Hot DOGs. This is in agreement with Assef et al. (2014) who found that Hot DOGs reside in overdense environments, as large as the CARLA clusters, but the angular clustering of the objects in the Hot DOG fields were smaller than in the CARLA fields.

Fig. 10 shows the fraction of the total number of serendipitous sources for the 30 SCUBA-2 maps found within cumulative circles of 0.25, 0.5, 0.75, 1.0, 1.25 and 1.5 arcmin from the *WISE* target. The expected fraction of the total number of serendipitous sources with no angular clustering, and the result from Jones et al. (2014) for 10 Hot DOGs that have no evidence of angular clustering on arcmin scales, is also plotted on Fig. 10. There is no hint of angular clustering of serendipitous sources around the *WISE*/radio-selected AGNs on scales less than 1.5 arcmin, despite the significantly greater average density of submm sources in the *WISE* fields as compared with blank-field surveys. Clustering of SMGs on larger scales than the extent of the SCUBA-2 field, could be expected because there is tentative evidence of clustering from previous submm studies on

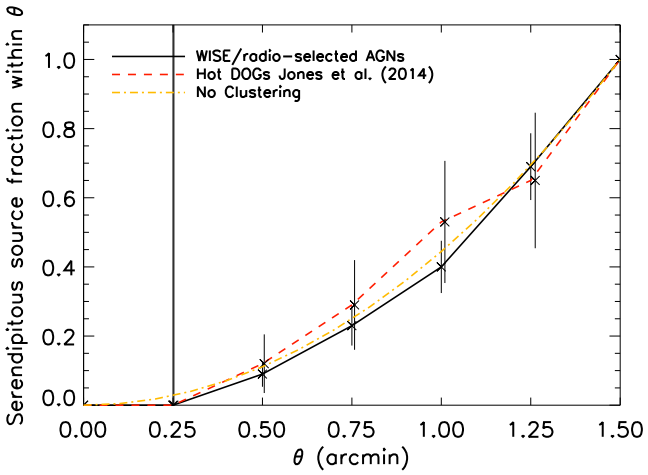

Figure 10. The cumulative fraction of the total number of serendipitous sources in each field within different radii of the *WISE* targets. The solid line shows the fields of the 30 *WISE*/radio-selected AGNs presented here. The dashed red line shows the 10 Hot DOGs from Jones et al. (2014). The yellow dash–dotted line shows the expected number of serendipitous sources if they are randomly located with no angular clustering. The beam size of SCUBA-2 at 850 μm is 14.5 arcsec; serendipitous sources cannot be detected within the beam.

scales up to ∼8 arcmin (Scoville et al. 2000; Blain et al. 2004; Greve et al. 2004; Farrah et al. 2006; Ivison et al. 2007; Weiß et al. 2009; Cooray et al. 2010; Scott et al. 2010; Hickox et al. 2012). Nevertheless, the lack of a clear two-point correlation signal is interesting, because SMG clustering observations can constrain the nature of the host haloes around SMGs (Cooray et al. 2010).

The average separation of a serendipitous source from the *WISE* central target is 58 arcsec, which is similar to the Hot DOG serendipitous sources, with an average separation from the *WISE* central target of 59 arcsec. This is consistent with Monte Carlo simulations of 1000 randomly placed serendipitous SMG sources from a central target, where the average separation was 60 arcsec. When looking at the separations between the serendipitous sources themselves, the average separation is 76 arcsec for *WISE*/radio-selected AGN serendipitous sources, 67 arcsec for Hot DOG serendipitous sources and 80 arcsec in 1000 randomly placed serendipitous SMG sources from Monte Carlo simulations. This would suggest that the serendipitous sources are not angularly clustered on these 1.5 arcmin scales.

6 DISCUSSION

6.1 *WISE*/radio-selected AGN SEDs and luminosities

The *WISE*/radio-selected AGN SEDs have bluer mid-IR sections than typical galaxies, while the SCUBA-2 observations show that they have relatively less submm emission than other galaxy SED templates: the detected *WISE*/radio-selected AGN targets' SCUBA-2 flux density is on average three times fainter than the bluest standard Polletta torus template. This leads to the suggestion that the *WISE*/radio-selected AGNs have less cold dust in the host galaxy and/or on the outer edge of the torus, and hence the torus could be denser, smaller and hotter than in the template. Alternatively, less submm emission could be due to an excess of mid-IR emission from the AGN as compared with the torus template (Wu et al. 2012; Tsai et al. 2014). The *WISE*/radio-selected AGN and

Hot DOG SEDs are both dominated by mid-IR emission; however, the *WISE*/radio-selected AGNs are submm fainter and mid-IR bluer.

The luminosities of the four detected targets (with a mean luminosity of $L_{8\,\mu\mathrm{m}-\mathrm{SCUBA2}} = 2.9 \times 10^{13}$ $\mathrm{L}_{\odot}$) are higher than those of typical SMGs, which have $L_{\mathrm{IR}} = 8.5 \times 10^{12}$ $\mathrm{L}_{\odot}$ (Chapman et al. 2005; Kovács et al. 2006), and DOGs, which have a mean luminosity $L_{\mathrm{IR}} = 9 \times 10^{12}$ $\mathrm{L}_{\odot}$ (Melbourne et al. 2012). High total IR luminosities were also found for the *WISE*/radio-selected AGNs from Lonsdale et al. (submitted) with a range of $L_{\mathrm{IR}} = 10^{12}$–$10^{13.55}$ $\mathrm{L}_{\odot}$. Hot DOGs had higher luminosities, with a mean luminosity of $L_{8\,\mu\mathrm{m}-\mathrm{SCUBA2}} = 5.3 \times 10^{13}$ $\mathrm{L}_{\odot}$ from Jones et al. (2014) and a mean luminosity of $L_{\mathrm{IR}} = 6.1 \times 10^{13}$ $\mathrm{L}_{\odot}$ from Wu et al. (2012). However, *WISE*-selected AGNs could be biased towards being the mid-IR brightest and rarest galaxies, because they were selected on the grounds of their bright mid-IR flux. Eight *WISE*-selected Lyman-alpha blobs (Bridge et al. 2013) were also found to be ultraluminous galaxies from *Herschel* data ($L_{\mathrm{IR}} = 2.3 \times 10^{13}$ $\mathrm{L}_{\odot}$), and included a wider range of mid-IR fluxes with no *WISE* colour selection cut. This indicates that galaxies with extremely red *WISE* colours have very luminous mid-IR properties.

WISE/radio-selected AGN SEDs are dominated by mid-IR emission and are very luminous compared to other galaxy populations, suggesting the galaxies are very active from either star formation or AGN activity, and have large amounts of obscuring hot dust, that could be due to merging galaxies.

6.2 *WISE*/radio-selected AGN environments

Comparing number counts of the serendipitous sources in the 30 *WISE*/radio-selected AGN fields with other submm surveys, implies there is an overdensity of SMGs in the 30 SCUBA-2 fields by factor of ∼4–6. This is consistent with finding *WISE*/radio-selected AGN in potentially overdense environments. This is an agreement with ALMA results of another subset of *WISE*/radio-selected AGNs from the same main sample (Lonsdale et al., submitted), who detected 23 serendipitous SMG sources in 17 out of 49 fields, which implies an overdensity factor of ∼10 compared to expected models and unbiased population number counts (Silva & Sajina 2014). There is double the overdensity of SMG serendipitous sources in the ALMA fields than our SCUBA-2 fields when compared to previous submm surveys, which is due to lower flux density limits (Silva & Sajina 2014, had deeper observations with rms noise level of ∼0.3–0.6 mJy beam^{-1}, which is lower than our rms noise level of ∼1.8–3.7 mJy beam^{-1}) and smaller spatial scales (Silva & Sajina 2014, observed ALMA fields with radius of 9 arcsec, which is smaller than our SCUBA-2 fields with radius of 90 arcsec). Silva & Sajina (2014) concluded that *WISE*/radio-selected AGNs reside in highly clustered environments, but further redshift data are needed to determine if they are in protocluster regions.

Our SMG overdensity results are also consistent with previous submm observations of HzRGs. The number of serendipitous sources around seven HzRGs in SCUBA maps were twice the expected number from other blank-field surveys (Stevens et al. 2003): our SMG overdensity is higher compared with other blank-field surveys, by a greater factor of ∼4–6. There appears to be no correlation between the redshift of the *WISE*/radio-selected AGN and the number of serendipitous sources found in the fields around it; however, the numbers here are only modest and more redshift data are needed to confirm this.

Stevens et al. (2003) detected on average one serendipitous source per HzRG field, compared to our average of three serendipitous sources per *WISE*/radio-selected AGN SCUBA-2 field. Our results in Fig. 11 and Table 4 agree that finding two 3σ SMG companions per field is likely: however, we find no fields with no 3σ serendipitous sources, and three 3σ serendipitous sources are more likely per field. This suggests that our SCUBA-2 fields and *WISE*/radio-selected sources have greater SMG overdensities compared with any previous surveys.

The Hot DOG fields had an SMG overdensity factor of ∼2–3 compared with blank-field submm surveys (Jones et al. 2014); however, these *WISE*/radio-selected AGNs have an even higher overdensity. 4 of the 10 Hot DOGs from Jones et al. (2014) have radio emission; W1603+2745 $S_{1.4\,\mathrm{GHz}} = 2.8 \pm 0.5$ mJy, W1814+3412 $S_{1.4\,\mathrm{GHz}} = 3.4 \pm 0.5$ mJy, W1835+4355 $S_{1.4\,\mathrm{GHz}} = 3.9 \pm 0.4$ mJy, W2216+0723 $S_{1.4\,\mathrm{GHz}} = 5.9 \pm 0.4$ mJy. However, the typical radio emission for Hot DOGs is 4 mJy, which is lower than *WISE*/radio-selected AGN value of 59 mJy. It suggests that the *WISE*/radio-selected galaxies which have radio emission are found in more overdense regions of the sky, compared to Hot DOGs with no or low radio emission. This is further evidence that AGN with radio-intermediate/loud emission reside in denser environments than radio-quiet AGN. This is not thought to be a selection bias, but rather indicates that RLAGN are located in more massive haloes

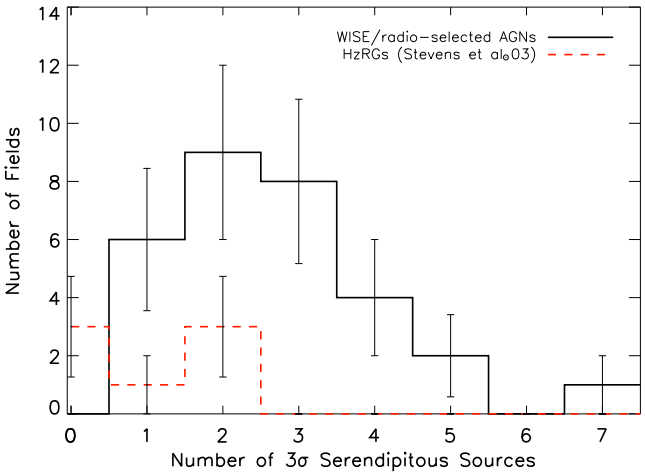

Figure 11. The black solid line is the number of serendipitous sources per SCUBA-2 field for all 30 *WISE*/radio-selected AGNs, the red dotted line is the SMG serendipitous number counts around HzRGs (fig. 4 from Stevens et al. 2003). A higher number of SMGs are found around the *WISE*/radio-selected AGNs than HzRGs; see also Table 4. The typical noise level of our 30 maps is ∼2.1 mJy beam^{-1}, which is comparable to ∼2.2 mJy beam^{-1} from Stevens et al. (2003).

Table 4. Number of serendipitous sources per SCUBA-2 field for all 30 WISE/radio-selected AGNs, Hot DOGs from Jones et al. (2014) and SMG serendipitous sources around HzRGs from Stevens et al. (2003).

Number of serendipitous sources	WISE/radio-selected AGNs	Hot DOGs	HzRGs
0	0	0	3
1	6	5	1
2	9	3	3
3	8	2	0
4	4	0	0
5	2	0	0
6	0	0	0
7	1	0	0

(Yates, Miller & Peacock 1989; Hill & Lilly 1991; Best, Longair & Roettgering 1998; Roche, Eales & Hippelein 1998; Best 2000; Donoso et al. 2010; Hatch et al. 2014). Our SMG overdensity could indicate that *WISE*/radio-selected AGNs are signposts of protocluster regions.

None of the serendipitous SMG sources in the *WISE*/radio-selected AGN and Hot DOG fields were detected in the NVSS or FIRST catalogues. However, 48 and 59 per cent of serendipitous SMG sources in the *WISE*/radio-selected AGN and Hot DOG fields, respectively, had counterparts in the AllWISE Source Catalog. All serendipitous sources detected around *WISE*/radio-selected AGNs were detected in the *W*1 band, 74 per cent in the *W*2 band, 10 per cent in the *W*3 band, and 0 per cent in the *W*4 band. All serendipitous sources detected around Hot DOGs were detected in the *W*1 band, 90 per cent in the *W*2 band, 20 per cent in the *W*3 band, and 0 per cent in the *W*4 band. Fig. 7 shows the *W*4 flux density versus SCUBA-2 850-μm flux density of the 39 serendipitous sources detected around the *WISE*/radio-selected AGNs that have *WISE* data, compared with *WISE*/radio-selected AGNs and Hot DOGs. From Fig. 7 it can be seen that the serendipitous sources are less bright in *W*4 and therefore, not as red in the mid-IR than *WISE*/radio-selected AGNs and Hot DOGs. This implies they are normal SMGs, that have $S_{850\,\mu m} > 2$ mJy, and are high-redshift galaxies with high IR luminosities believed to be from starburst activity, but are faint in optical and near-IR wavelengths (Ivison et al. 1998; Eales et al. 1999; Barger, Cowie & Richards 2000; Smail et al. 2000; Chapman et al. 2001; Blain et al. 2002; Ivison et al. 2002, 2004; Pope et al. 2006). Most of the serendipitous SMG sources will be at a similar redshift ($1 \leq z \leq 3$) to the *WISE*/radio-selected AGNs (Karim et al. 2013), but some will be inevitably unassociated in redshift.

These *WISE*/radio-selected AGNs appear to be very powerful AGN that have more mid-IR emission, and mid-IR opacity than AGN in standard galaxy templates. Therefore, the *WISE*/radio-selected AGNs might be experiencing the most powerful AGN feedback possible and could be an obscured AGN-dominated short evolutionary phase of merging galaxies, for example the Hot DOG target W1814+3412 has three components of the same redshift and within 50 kpc of each other (Eisenhardt et al. 2012). The *WISE*/radio-selected AGNs also appear to reside in intriguing many-arcmin-scale overdensities of very luminous, dusty sources.

WISE/radio-selected AGNs have lower submm flux densities, higher radio emission, lower redshifts and denser environments than Hot DOGs. These could be due to Hot DOGs having a higher typical redshift, and were selected to be mid-IR redder. *WISE*/radio-selected AGNs and Hot DOGs appear to be consistent with a transient AGN-dominated phase of the major merger theory, but starburst activity cannot be ruled out. The *WISE*/radio-selected AGNs appear to be signposts of overdense regions of active, luminous and dusty galaxies.

7 SUMMARY

The results from SCUBA-2 850 μm observations of 30 *WISE*/radio-selected, high-redshift, luminous, dusty AGNs are as follows.

(i) The 30 *WISE*/radio-selected AGNs have SEDs that are not well fitted by the current AGN templates (see Fig. 5); the best fitting is the Polletta torus (Polletta et al. 2007) template.

(ii) The detected *WISE*/radio-selected AGNs have less cold dust than the Polletta torus template, which could be because there is less cold dust in the host galaxy, and/or the outer scale of the AGN torus in the *WISE*/radio-selected AGNs are smaller. Alternatively there could be more intense mid-IR emission from hotter inner regions (Wu et al. 2012).

(iii) Despite being observed over a wide redshift range, the 10 *WISE*/radio-selected AGNs with known redshift data show uniform submm to mid-IR ratios. The highest redshift, most luminous targets, could thus have hotter dust temperatures than assumed in the templates. However, the number of targets with known redshifts is currently only modest (10) and the selection of the targets is sensitive to redshift, owing to very red *WISE* colours.

(iv) The detected *WISE*/radio-selected AGNs have high IR luminosities, $L_{8\,\mu m\text{–SCUBA2}} \geq 10^{13}$ $L_{\odot}$, confirming they are HyLIRGs. These are conservative values as any pronounced peak of the SED would increase these further. The undetected *WISE*/radio-selected AGNs have upper limit luminosities that are consistent with LIRGs.

(v) The luminosity of an underlying extended star-forming galaxy cannot exceed a luminosity ∼4 per cent (for a cool spiral galaxy template) or ∼10 per cent (for a warmer ULIRG-like galaxy template) as compared with the submm-detected typical *WISE*/radio-selected AGNs luminosity. Our SCUBA-2 observations confirm that *WISE*/radio-selected AGNs are a mid-IR dominated population.

(vi) When comparing the submm galaxy counts of the 30 1.5-arcmin-radius SCUBA-2 maps observed here to blank-field surveys, there is an overdensity of SMGs on this scale by a factor 4–6, but no evidence for any angular clustering within these fields.

(vii) There is an SMG overdensity of order ∼2 when comparing *WISE*/radio-selected AGNs to Hot DOGs, and suggests that *WISE*/radio-selected AGNs are signposts of overdense regions of active, luminous and dusty galaxies in the sky.

(viii) *WISE*/radio-selected AGNs and Hot DOGs appear to be consistent with a transient AGN-dominated phase of the major merger theory, but starburst activity cannot be ruled out.

ACKNOWLEDGEMENTS

The authors would like to thank the anonymous referee for his/her comments and suggestions, which have greatly improved this paper.

SFJ gratefully acknowledges support from the University of Leicester Physics & Astronomy Department. This publication makes use of data products from the *WISE*, which is a joint project of the University of California, Los Angeles, and the Jet Propulsion Laboratory/California Institute of Technology, funded by the National Aeronautics and Space Administration.

The James Clerk Maxwell Telescope has historically been operated by the Joint Astronomy Centre on behalf of the Science and Technology Facilities Council of the United Kingdom, the National Research Council of Canada and the Netherlands Organization for Scientific Research. Additional funds for the construction of SCUBA-2 were provided by the Canada Foundation for Innovation. The programme IDs under which the data were obtained were M12BU07 and M13BU02.

RJA was supported by Gemini-CONICYT grant number 32120009.

REFERENCES

Assef R. J. et al., 2013, ApJ, 772, 26
Assef R. J. et al., 2014, preprint (arXiv:1408.1092)
Barger A. J., Cowie L. L., Richards E. A., 2000, AJ, 119, 2092
Barnes J. E., Hernquist L., 1992, ARA&A, 30, 705
Becker R. H., White R. L., Helfand D. J., 1995, ApJ, 450, 559

Best P. N., 2000, MNRAS, 317, 720
Best P. N., Longair M. S., Roettgering H. J. A., 1998, MNRAS, 295, 549
Blain A. W., Smail I., Ivison R. J., Kneib J.-P., Frayer D. T., 2002, Phys. Rep., 369, 111
Blain A. W., Chapman S. C., Smail I., Ivison R., 2004, ApJ, 611, 725
Borys C., Scott D., Chapman S., Halpern M., Nandra K., Pope A., 2004, MNRAS, 355, 485
Bridge C. R. et al., 2012, preprint (arXiv:1205.4030)
Bridge C. R. et al., 2013, ApJ, 769, 91
Casey C. M. et al., 2013, MNRAS, 436, 1919
Chapin E. L., Berry D. S., Gibb A. G., Jenness T., Scott D., Tilanus R. P. J., Economou F., Holland W. S., 2013, MNRAS, 430, 2545
Chapman S. C., Richards E. A., Lewis G. F., Wilson G., Barger A. J., 2001, ApJ, 548, L147
Chapman S. C., Blain A. W., Smail I., Ivison R. J., 2005, ApJ, 622, 772
Chapman S. C., Blain A., Ibata R., Ivison R. J., Smail I., Morrison G., 2009, ApJ, 691, 560
Condon J. J., Cotton W. D., Greisen E. W., Yin Q. F., Perley R. A., Taylor G. B., Broderick J. J., 1998, AJ, 115, 1693
Cooray A. et al., 2010, A&A, 518, L22
Coppin K. et al., 2006, MNRAS, 372, 1621
Cutri R. M. et al., 2003, VizieR Online Data Catalog, 2246, 0
de Grijp M. H. K., Lub J., Miley G. K., 1987, A&AS, 70, 95
Dempsey J. T. et al., 2013, MNRAS, 430, 2534
Donley J. L. et al., 2012, ApJ, 748, 142
Donoso E., Li C., Kauffmann G., Best P. N., Heckman T. M., 2010, MNRAS, 407, 1078
Donoso E., Yan L., Stern D., Assef R. J., 2014, ApJ, 789, 44
Eales S., Lilly S., Gear W., Dunne L., Bond J. R., Hammer F., Le Fèvre O., Crampton D., 1999, ApJ, 515, 518
Eisenhardt P. R. M. et al., 2012, ApJ, 755, 173
Fabian A. C., 2012, ARA&A, 50, 455
Falder J. T. et al., 2010, MNRAS, 405, 347
Fanti C. et al., 2000, A&A, 358, 499
Farrah D. et al., 2001, MNRAS, 326, 1333
Farrah D. et al., 2006, ApJ, 641, L17
Farrah D. et al., 2012, ApJ, 745, 178
Galametz A. et al., 2010, A&A, 522, A58
Galametz A. et al., 2012, ApJ, 749, 169
Geach J. E. et al., 2013, MNRAS, 432, 53
Giacintucci S., Venturi T., Murgia M., Dallacasa D., Athreya R., Bardelli S., Mazzotta P., Saikia D. J., 2007, A&A, 476, 99
Gilli R., Comastri A., Hasinger G., 2007, A&A, 463, 79
Greve T. R., Ivison R. J., Bertoldi F., Stevens J. A., Dunlop J. S., Lutz D., Carilli C. L., 2004, MNRAS, 354, 779
Gruppioni C. et al., 2008, ApJ, 684, 136
Hatch N. A. et al., 2014, MNRAS, 445, 280
Hickox R. C. et al., 2009, ApJ, 696, 891
Hickox R. C. et al., 2012, MNRAS, 421, 284
Hill G. J., Lilly S. J., 1991, ApJ, 367, 1
Holland W. S. et al., 2013, MNRAS, 430, 2513
Hopkins P. F., Hernquist L., Cox T. J., Di Matteo T., Robertson B., Springel V., 2006, ApJS, 163, 1
Hopkins P. F., Hernquist L., Cox T. J., Kereš D., 2008, ApJS, 175, 356
Ivison R. J., Smail I., Le Borgne J.-F., Blain A. W., Kneib J.-P., Bezecourt J., Kerr T. H., Davies J. K., 1998, MNRAS, 298, 583
Ivison R. J. et al., 2002, MNRAS, 337, 1
Ivison R. J. et al., 2004, ApJS, 154, 124
Ivison R. J. et al., 2007, MNRAS, 380, 199
Jarrett T. H. et al., 2011, ApJ, 735, 112
Jones S. F. et al., 2014, MNRAS, 443, 146
Karim A. et al., 2013, MNRAS, 432, 2
Keel W. C., de Grijp M. H. K., Miley G. K., Zheng W., 1994, A&A, 283, 791
Kellermann K. I., 1974, in Verschuur G. L., Kellermann K. I., van Brunt V., eds, Radio Galaxies and Quasars. Springer-Verlag, Berlin, p. 320
Kovács A., Chapman S. C., Dowell C. D., Blain A. W., Ivison R. J., Smail I., Phillips T. G., 2006, ApJ, 650, 592
Krolik J. H., Begelman M. C., 1988, ApJ, 329, 702
Lacy M. et al., 2004, ApJS, 154, 166
Lonsdale C. J., Lonsdale C. J., Smith H. E., Diamond P. J., 2003, ApJ, 592, 804
Lonsdale C. J., Farrah D., Smith H. E., 2006, Astrophysics Update 2. Springer-Verlag, Berlin, p. 285
Low F. J., Cutri R. M., Huchra J. P., Kleinmann S. G., 1988, ApJ, 327, L41
Mateos S., Alonso-Herrero A., Carrera F. J., Blain A., Severgnini P., Caccianiga A., Ruiz A., 2013, MNRAS, 434, 941
Mayo J. H., Vernet J., De Breuck C., Galametz A., Seymour N., Stern D., 2012, A&A, 539, A33
Melbourne J. et al., 2012, AJ, 143, 125
Neugebauer G. et al., 1984, ApJ, 278, L1
Polletta M. d. C. et al., 2006, ApJ, 642, 673
Polletta M. et al., 2007, ApJ, 663, 81
Polletta M., Weedman D., Hönig S., Lonsdale C. J., Smith H. E., Houck J., 2008, ApJ, 675, 960
Pope A. et al., 2006, MNRAS, 370, 1185
Roche N., Eales S., Hippelein H., 1998, MNRAS, 295, 946
Sacchi N. et al., 2009, ApJ, 703, 1778
Sanders D. B., Mirabel I. F., 1996, ARA&A, 34, 749
Sanders D. B., Soifer B. T., Elias J. H., Madore B. F., Matthews K., Neugebauer G., Scoville N. Z., 1988, ApJ, 325, 74
Schweizer F., 1998, in Kennicutt R. C., Jr, Schweizer F., Barnes J. E., Friedli D., Martinet L., Pfenniger D., eds, Galaxies: Interactions and Induced Star Formation: Saas-Fee Advanced Course 26. Springer, Berlin, p. 105
Scott S. E., Dunlop J. S., Serjeant S., 2006, MNRAS, 370, 1057
Scott K. S. et al., 2010, MNRAS, 405, 2260
Scoville N. Z. et al., 2000, AJ, 119, 991
Seymour N. et al., 2012, ApJ, 755, 146
Silva A. L., Sajina A., 2014, Am. Astron. Soc. Meeting Abstr., 224, #222.13
Smail I., Ivison R. J., Owen F. N., Blain A. W., Kneib J.-P., 2000, ApJ, 528, 612
Spinoglio L., Malkan M. A., 1989, ApJ, 342, 83
Stern D. et al., 2005, ApJ, 631, 163
Stern D. et al., 2012, ApJ, 753, 30
Stevens J. A. et al., 2003, Nature, 425, 264
Stevens J. A., Jarvis M. J., Coppin K. E. K., Page M. J., Greve T. R., Carrera F. J., Ivison R. J., 2010, MNRAS, 405, 2623
Tommasin S., Spinoglio L., Malkan M. A., Fazio G., 2010, ApJ, 709, 1257
Tsai C.-W. et al., 2014, preprint (arXiv:1410.1751)
Umehata H. et al., 2014, MNRAS, 440, 3462
Varenius E., Conway J. E., Martí-Vidal I., Aalto S., Beswick R., Costagliola F., Klöckner H.-R., 2014, A&A, 566, A15
Veilleux S., Kim D.-C., Sanders D. B., 2002, ApJS, 143, 315
Venemans B. P. et al., 2007, A&A, 461, 823
Volonteri M., Natarajan P., Gültekin K., 2011, ApJ, 737, 50
Weiß A. et al., 2009, ApJ, 707, 1201
Wright E. L. et al., 2010, AJ, 140, 1868
Wu J. et al., 2012, ApJ, 756, 96
Wylezalek D. et al., 2013, ApJ, 769, 79
Wylezalek D. et al., 2014, ApJ, 786, 17
Yan L. et al., 2005, ApJ, 628, 604
Yates M. G., Miller L., Peacock J. A., 1989, MNRAS, 240, 129

This paper has been typeset from a TEX/LATEX file prepared by the author.